Sea ice remote sensing, thickness profiling, and ice and snow analyses during Polarstern cruise Ark 19/1 / CryoVex2003 in the Barents Sea and Fram Strait, February 28 – April 24, 2003: Cruise report

Authors: C. Haas, V. Alexandrov, S. Kern, J. Lieser, J. Lobach, T. Martin, A. Pfaffling, S. Willmes

Table of contents

1. Outline (C. Haas)

The main goal of the geophysical sea ice work during Ark 19/1 was the determination of representative sea ice thickness distributions in Storfjord and the Barents Sea, as well as in Fram Strait, and the validation of a range of different satellite remote sensing data.

In Storfjord and the Barents Sea, the data were acquired to obtain estimates of the ice production in the Storfjord Polynja, as an independent assessment of oceanographic and meteorological salt and energy budget observations.

In Fram Strait, the geophysical field work was part of the CryoSat Validation Experiment CryoVex 2003 co-ordinated by the European Space Agency ESA. Coincident, synchronous helicopter flights were carried out with a Danish Twin Otter fixed-wing aircraft equipped with a synthetic aperture radar altimeter resembling the new-generation SIRAL radar altimeter on board ESA's upcoming CryoSat mission in 2004. CryoSat is dedicated to observe the ice thickness of the earth's land and sea ice masses.

Sea ice thickness measurements were complemented by a number of other observations including ice coring and snow sampling, visual ice observations and satellite image acquisition. The work was carried out in the framework of and supported by three EU projects GreenICE, SITHOS, and IRIS. Within these projects, real-time Envisat, ERS and QuickScat satellite imagery were transmitted to the ship as navigational support and for validation purposes by Norwegian (Nansen Environmental and Remote Sensing Center, Bergen) and Danish (Danish Technical University, Lyngby) partners.

2. General ice conditions

Hourly, standardised visual ice observations were performed in a joint effort by all 16 sea ice scientists during daylight hours when the ship was moving through ice. In total, 279 observations were performed.

On board, all observations and photographs were typed into Excel spreadsheets and linked html pages, and will be made available on the www after return to Bremerhaven.

2.1 Storfjord and Barents Sea (C. Haas)

A diffuse ice edge with bands of pancake brash was crossed at about 8:00 UTC on March 6 between Björnøya and Svalbard (see cruise track; Fig.SEAICE.1). From there, the ship passed in 70 to 90 % ice concentration with small thin floes < 20 m diameter to the southern tip of Svalbard. There, very heavy ice conditions were met requiring continuous ramming, lasting until March 21, when Storfjorden was left into the Barents Sea. Between March 7 and March 21, in outer Storfjorden Polarstern sailed in almost always 100 % ice concentration, with 0.4 to 1.8 m thick small floes (typically < 30 m diameter) covered with 20 to 30 cm of snow, embedded in heavily ridged and rubbled ice. As was interpreted from satellite radar imagery (Figs. SEAICE.1, SEAICE.2) and ice core analyses (Section SEAICE.6), this ice was a mixture of second-year and multiyear floes from the Arctic Ocean, with deformed first-year ice in between.

Only few cracks and narrow leads led to the inner Storfjord region, where grey ice with thin or no snow prevailed and where Polarstern made good progress. As can be seen on the satellite images, this region of young and first-year ice formed in Storfjorden extended all along the western margin of the fjord. However, CTD work required a return into heavy ice soon again.

No opening of a large polynja occurred during our study. As can be seen on the near infrared image in Figure SEAICE.3, open water and thin ice were confined to a narrow zone along the northern and north eastern coasts. However, as outlined above, by the end of March ice formed in Storfjorden could be tracked southward to the southern tip of Svalbard.

After March 21, in the Barents Sea with ice concentrations of 90 to 100% big floes (100-1000 m diameter) with less ridging but 20 to 30 cm snow were encountered. After March 24, fracturing due to ocean swell was observed, and bigger polynjas inside the closed pack covered with new ice and extensive amounts of frost flowers. After this, the marginal ice zone with heavy swell was left through a very diffuse ice edge into the open Barents Sea on March 26 to sail to Longyearbyen. On March 28, close to Svalbard ice exported from the Storfjord was encountered in the West Spitzbergen Current. Ice concentration was as high as 90 %, with small but thick deformed and snow covered floes.
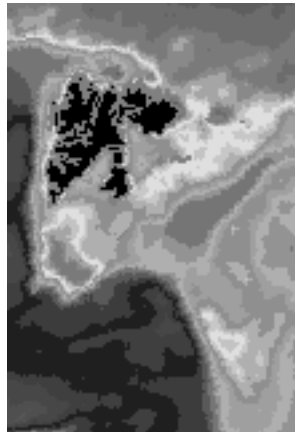
Figure SEAICE.1: QuickScat HH backscatter image of Svalbard and the Barents Sea from March 06. 2003. Dark tones represent low backscatter, bright tones represent high backscatter. The image shows the flow lines of older ice form the Arctic Ocean and first year ice formed leeward of Franz Josef Land and in Storfjorden. Image courtesy of L. Toudal, DTU.

Figure SEAICE.2: Mosaic of ERS and Envisat SAR images acquired between March 17 and 21. Superimposed are the coastline of Svalbard and the actual cruise track until March 21 as well as planned stations. Different textures of second/multiyear ice and first-year ice can be seen and compared to Figure SEAICE.1. Image courtesy K. Kloster, NERSC.

Figure SEAICE.3: NOAA-AVHRR near infrared image of Storfjorden received on board on March 19 (Section SEAICE.3.1), showing the distribution of polynjas and thin ice areas, as well as the first-year ice exported from Storfjord.
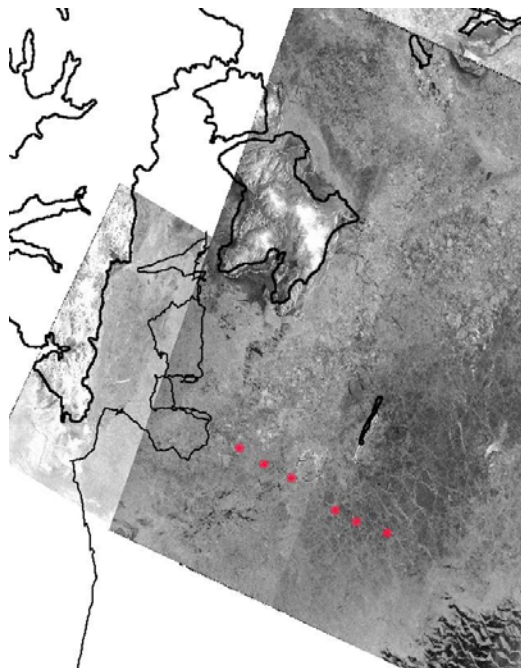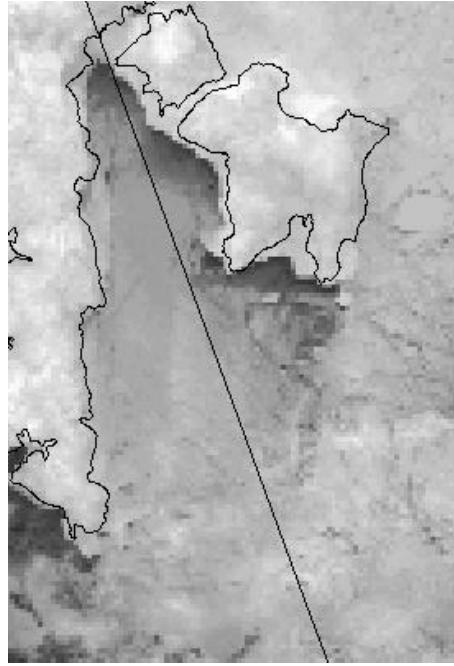
2.2 Northwest of Svalbard (S. Kern)

On March 29 the ship arrived in Isfjorden which was covered up to 90% with nilas and grey-ice and some smashed first-year ice. During and after leave of Isfjorden nilas and pancakes where encountered until March 30, 6 UTC, when last bands of almost completely melted brash ice were observed at 78°55'N, 7°35'E, while steaming westward. On March 31, steaming northeastward, the ship arrived at the ice edge at 80°05'N, 11°18'E. In between, isolated, almost completely melted second-year and multiyear ice floes were observed (e.g. at 79°04'E, 4°18'E); later, i.e. further north (around 79°50'N, 9°01'E and further east) bands of first-year ice floes and open water were observed. Typical ice (snow) thickness was 0.70 m (0.1-0.2 m) at the ice edge.

The ice coverage encountered during the next days until arrival at the drift station ice floe on April 6 at 81°54'N, 9°28'E, was between 90 and 100% comprising mostly first-year/second-year and multiyear ice floes (on average 100-200 m in diameter). These floes were separated by leads which were between 50 and 500 m (2000 m) wide. The leads were typically covered with nilas, grey, and grey-white ice, often covered by dense frost flower mats. Through these leads which can be seen in figures SEAICE.5 and SEAICE.8 quite clearly the ship was navigated to the drift station ice floe. Ice thickness in leads varied between 0.03 and 0.20 m whereas it was between 0.80 to 2.00 m otherwise. Observed snow depths ranged from 0.05 to 0.30 m on thick ice. Notable rubble fields (up to 30% of the total ice coverage) were observed on April 1 at around 80°26'N, 12°49'E. Typical ridge height and spacing was 1 m and 100 m, respectively. On the way to the drift station ice floe, the ship was stuck two times; the first time on April 3 at 80°42'N, 13°14'E for about six hours in a floe with a 3 m high ridge; the second time on April 4/5 for about 30 hours in a 0.8-1.2 m thick first-year ice floe which itself was stuck between two multiyear ice floes.

After leaving the drift station ice floe on April 18, at 81°38'N, 9°59'E, still heavy ice conditions were encountered with 90 to 100% of first-year/second-year and multiyear ice

floes with an average diameter of 200 m, a snow depth of 0.15 to 0.30 m and average ridge height and spacing of 1 m and 100 m, respectively. Between these floes dark and light nilas was observed - almost without frost flowers. Rubble fields amounted up to 20% of the total ice cover. Between April 19 and 20, i.e. 81°15'N, 10°33'E and 80°35'N, 10°20'E, ice concentrations decreased to between 80 and 95%. The ice coverage comprised 1 to 2 m thick first-year/second-year and multiyear ice. Typical floe sizes decreased to between 20 and 50 m and looked like as if broken by recent swell activity. Floes were separated by brash ice rather than nilas. The ice type changed to mainly first-year ice around 80°19'N, 7°38'E with a decrease of the typical ice (snow) thickness to 0.40 to 0.60 m (0.05 to 0.10 m). Further to the southwest (80°12'N, 7°31'E) a mixture of such first-year ice and up to 2 m thick second-year/multiyear ice was observed together with some nilas and grey-ice as well as open water. Ice concentrations dropped to 60 to 90%. On April 21 at about 12 UTC the ship arrived in open water at about 79°20'N, 3°54'E, after steaming through 20 to 60% ice coverage with melting first-year ice.

3. Remote Sensing

3.1 NOAA-AVHRR imagery (J. Lieser, C. Haas)

The satellite receiving system installed onboard RV POLARSTERN receives data from the polar orbiting NOAA-Satellites (National Oceanographic and Atmospheric Associatian, USA) NOAA-12, NOAA-15, NOAA-16 and NOAA-17. The satellites operate in a near-polar sun-synchronous orbit at a height of about 850 km. During the two legs of cruise ARK 19/1 more than 1000 passes have been captured and post-processed. The HRPT-Telemetry (High Resolution Picture Transmission) includes scans of the AVHRR-Sensor (Advanced Very High Resolution Radiometer) as well as information of the DCS-Platform (Data Collecting and Positioning System). AVHRR is a five channel radiometer operating in the visible (two channels) and near infrared (three channels) wavelength range with a nadir resolution of about 1.1 km. DCS receives environmental and GPS data (Global Positioning System) of either stationary or moving platforms, like ARGOS-buoys deployed on ice floes prior to the second leg of the cruise for meteorological data collection by the Met-Group from the University of Hamburg (see section xxx). Positions and data of this buoy array were monitored via DCS and one buoy was successfully recovered after the drift-station.

More than 350 passes have been archived for further post processing. This will include exact geolocation of image data and analysis of information from the infrared channels in combination with data collected by the KT-15 infrared thermometer operated synchronously with SIMS (Section SEAICE.4.1.2) in front of the ship. Only in cloud free scenes imagery was used for real time information about ice conditions around the ship and as a guiding information for Polarsterns bridge. Several SAR images (see Section SEAICE.3.2) were also used to support the scientific cruise leader and the ship's bridge for decision making on the way through the ice. Especially while looking for an appropriate ice floe for the drift-station north of Svalbard and for finding a feasible way getting there and back again those images proved to be very helpful information.

A typical AVHRR infrared image is shown in Figure SEAICE.4. Bright values indicate low temperatures, dark values correspond to higher temperatures. The scene was received on March 25. 2003 at 02:36 UTC from NOAA-16. It covers the Fram Strait, Svalbard, the Barents Sea, and the straits to Franz-Josef-Land, where a quite closed pack ice cover is present. Storfjord and the western Barents Sea appear ice covered as well but with smaller floes the signature is more diffuse. The darker values in the eastern part of Storfjord at the

west coast of Edgeøya and Barentsøya indicate a polynja region with very thin ice cover or even open water. Because of the comparably warm water which is either directly exposed to the atmosphere or covered only with a very thin ice layer this region appears with darker tone. The black cross denotes the position of RV Polarstern at receiving time some days before the end of the first leg of the cruise.

Figure SEAICE.5 shows an example of typical late winter / early spring sea ice conditions for the Fram Strait region. The image covers the same geographical area as Figure SEAICE.4. It was received on April 05. 2003 at 08:19 UTC from NOAA-15. Again, large ice floes are clearly visible between Svalbard and Greenland. The ice edge follows approximately a line from 80 N 10 E to 75 N 10 W. South of this line a cold air outbreak from the North forms a typical cloud pattern over the open ocean. The Barents Sea appears to be mostly cloudy, but some ice is visible through the thin low cloud cover. Again the arched dark features north of 80 N show thin ice covers or open water mainly in lee of larger ice floes. Those fractures were used both on the way into the ice towards the location of the drift-station and back out of the ice towards the Hausgarten region (see Section xxxIngoScheewe). The black cross denotes the position of RV Polarstern at receiving time.
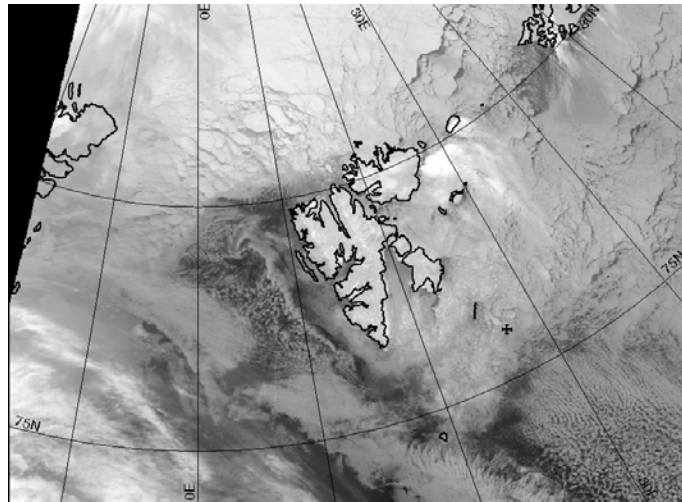

Figure SEAICE.4: Image received on March 25th 2003 at 02:36 UTC from NOAA-16. The scene shows the area around Svalbard as seen from AVHRR channel 4.

Figure SEAICE.5: Image received on April 5th 2003 at 08:19 UTC from NOAA-15. The scene shows the area around Svalbard as seen from AVHRR channel 4.

3.2 Synthetic Aperture Radar (SAR) images. (V.Alexandrov, C. Haas, J. Lieser)

SAR images from different satellites have been ordered to cover the ARK 19 study regions: ENVISAT, RADARSAT, and ERS SAR. Some of these images have been acquired and archived at the Tromsoe Satellite Station (TSS), and some of them have been acquired in near-real time and transmitted to Polarstern via INMARSAT and IRIDIUM communication systems. Onboard Polarstern SAR images were used both for navigation purposes and for planning field work. Radar signatures of different sea ice types and features have been investigated by means of comparison with subsatellite sea ice observations. ERS SAR scenes cover areas of 100 x 100 km with a resolution of 25 m.

Five ERS-2 SAR scenes were acquired onboard Polarstern during the first leg of the expedition. The first two images, dated February 27 and March 2, covering the area of Storfjord, were used for estimating sea ice conditions. The first ENVISAT ASAR image, covering Storfjord area, was received on March 14. This image was immediately used for navigation purposes and planning field work. This image is shown in Figure SEAICE.6.
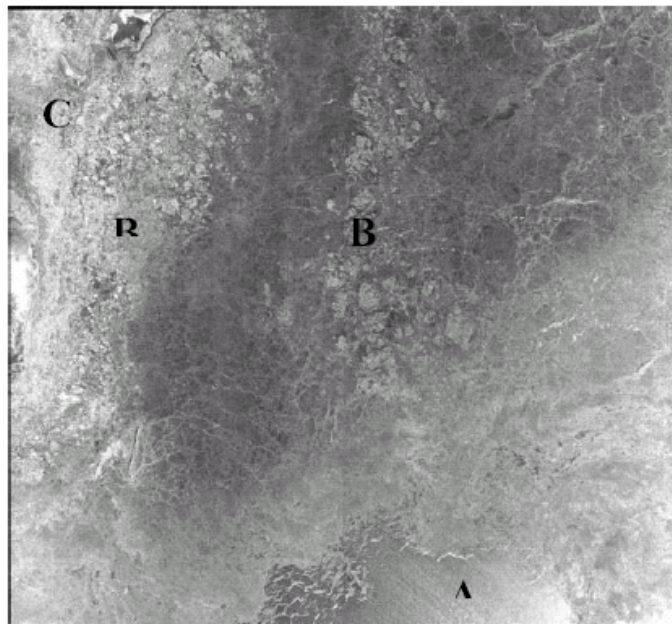

Figure SEAICE.6: ENVISAT ASAR image for March 14, covering the area south and east of Storfjorden.

Ice edge position can be seen in the lower right part of this image (area A). The multiyear sea ice, which is imported from the central Arctic is evident in two areas, marked by B, with light tone, and rather level first-year ice located between these two areas is shown with dark tone. Rather bright image tone in Storfjorden (area C) is due to significant surface roughness.

Three ERS-2 SAR images, acquired on March 16, 18, and 19 for the Storfjorden and eastward of it in the Barents Sea, were used for estimating sea ice conditions in this area, as well as ENVISAR ASAR image, dated March 20. Another ASAR for the same date covered Storfjorden and area west of Svalbard. The area west of Svalbard was also covered with ENVISAT image for March 25. In both these images a stripe of ice along the coast of Svalbard is clearly evident as well as young ice in Isfjorden and ice edge position north of the archipelago. From ASAR image for March 26 ice edge position in the north western part of the Barents Sea and Storfjorden can be easily determined. The ENVISAT ASAR image for March 28 covered Svalbard and area westward of it in the time when Polarstern approached

Isfjorden. Near simultaneous in situ sea ice observations were compared with signatures of different new and young ice types in Isfjorden, and also in the area west of it.

After March 29 the second leg of the cruise to the north of Svalbard began. This area is characterized by significantly more complicated sea ice conditions than in the Barents Sea and remote sensing data were particularly important. ENVISAT ASAR image for March 30 covered this area and provided a possibility to estimate sea ice conditions there to plan how we can approach the needed area. This image is shown in Figure SEAICE.7.

A diffuse ice edge is evident in area A. A mixture of first-year and multiyear ice persists in the transient area between ice edge and multiyear ice to the north. A number of giant multiyear ice floes are located to the north of Svalbard, and one of these floes is marked with B. They are shown with relatively bright tone, caused by volume scattering of radar signal in upper layer of multiyear ice, which is saturated with air bubbles. Fractures of different width, covered with new or young ice, are situated between these ice floes (in area C, for example). Their tone can vary from dark to bright, but in any case they could be detected among surrounding ice. Using these fractures a further route of the expedition was chosen. During the drifting stage SAR images have not been received onboard the Polarstern due to communication problems. Only in the final stage one SAR images was used for selecting return way.

Figure SEAICE.8 shows a Radarsat Narrow Swath image from April 04, covering some of Figure SEAICE.7 and adjacent regions to the west. Svalbard is in the right margin. Some features can be identified on both images, enabling tracking of floes and detection of changes. Studies of ice signatures with different polarizations (Envisat: VV, Radarsat: HH) can also be performed. Three Radarsat images (March 26 and April 04 and 14) were purchased as navigational support for Polarstern. Unfortunately though, image ordering was not flexible enough so that the drift floe is not covered by any of the Radarsat imagery. However, some HEM flights are well within the images.
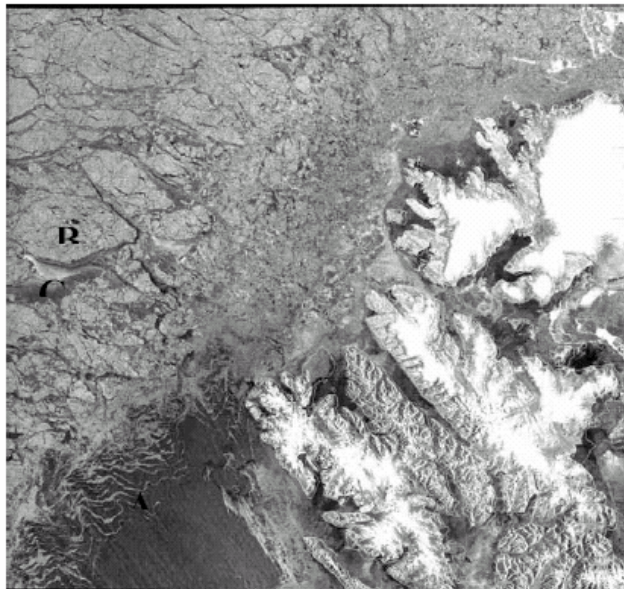

Figure SEAICE.7: ENVISAT ASAR image for March 30, covering sea ice northward of Svalbard.
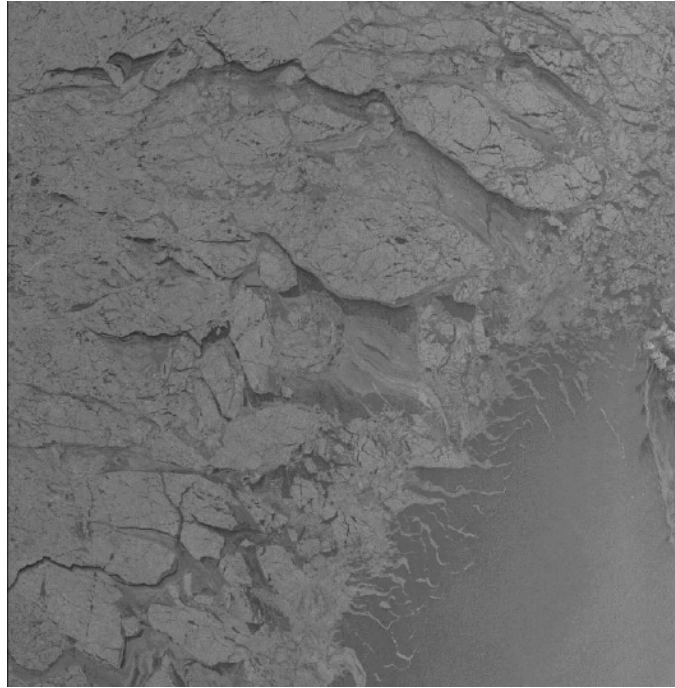
Figure SEAICE.8: Radarsat Narrow Swath SAR image from April 04, showing Fram Strait northwest of Svalbard.

3.3 Low resolution satellite data (C. Haas)

As part of the GreenICE project, different ice products derived from passive microwave SSM/I and QuickScat Scatterometer were transmitted by email to Polarstern by the Danish Technial University (DTU, courtesy Leif Toudal) on a daily basis. All imagery was installed with a special browser on the ships public computer network and was accessible by all cruise participants. The data was very useful for estimating the overall ice situation, and in particular the ice edge position. Moreover, QuickScat provided some ice type information (see Figure SEAICE.1 above) which was essential in guiding and interpreting the airborne and ground ice property measurements.

3.4 Helicopter Scatterometer Measurements (HELISCAT; S. Kern)

A. The instrument:

The HELISCAT is a helicopter-based Scatterometer designed to measure quasi-simultaneous the surface radar backscatter at five different frequencies in the microwave frequency range (1.0, 2.4, 5.3, 10.0, 15.0 GHz, i.e. in the L-, S-, C-, X-, and Ku-Band, respectively), at HH-, VV-, and cross-polarization. It consists of the SCAT (five pulsed superheterodyne Doppler-Scatterometers) which generates, transmits and receives the signal, a parabolic broad-band dish antenna (1 m in diameter), a gyro, which measures pitch and roll of the helicopter, and a steering unit which controls the power supply, transmit and receive cycles, and which directs the signal to a tape-recorder for data storage. The gyro and the SCAT are mounted in an antenna rack which itself is mounted inside the helicopter. The antenna is aft-looking and is mounted outside the helicopter on an arm of the antenna rack which can be tilted during the flight so that the incidence angle can be varied between 20 and 70 degrees. A CCD-Camera is mounted on the same arm and is used together with a timer, a monitor and a video-recorder to observe the different surface types within the footprint of the antenna. This equipment is mounted together with the tape recorder, the steering unit, and two filters and amplifiers in a rack which is also placed inside the helicopter. The HELISCAT can be used from flight

altitudes between about 50 and 1000 m. The size of the elliptical footprint depends on frequency, incidence angle and flight altitude and takes across-flight track values between about 3 m for Ku-Band (beamwidth: 0.9°) and about 50 m for L-Band (beamwidth: 13.6°) at a flight altitude of 150 m. The sampling rate is 100 µs which ensures a continuous data acquisition along the flight track.

The measured parameter is the so-called normalised radar cross section (NRCS) which is roughly a measure for the amount of energy which is backscattered into the direction of the radar. The radar backscatter (or NRCS) of sea ice is determined by many different factors and properties: incidence angle, frequency (wavelength), and polarisation, snow properties such as wetness, density, grain size, and sea ice properties such as porosity, salinity, grain size, and roughness on the mm- to cm-scale. Young ice formed, for instance, under quiet conditions is level and has rather a low radar backscatter because its surface roughness is quite small which causes only a small amount of energy to be backscattered into the direction of the radar. In contrast, young ice formed as pancakes, i.e. under windy conditions, shows high NRCS-values due to the mm- to cm-scale rims on its surface which cause a fair amount of surface scattering. Multiyear ice also has a high radar backscatter. The reason for this is twofold. At first this is due to a larger surface roughness compared to level sea ice. And secondly this is caused by many air pockets entrapped in the upper centimeters of the ice, which cause volume scattering.

The influence of snow on the backscatter measurements can be neglected as long as the snow is dry and free of ice layers with grain sizes that match the radar wavelength. In this case the radar penetrates the snow layer and the measured NRCS reflects the properties of the snow-ice interface and of the ice layer some centimeters thick below. In case of a wet snow surface, most of received energy stems from the upper millimeters to centimeters of the snow cover. In case of an icy layer of large-grained snow crystals buried in otherwise fine-grained dry snow, the measured NRCS-values are determined by the structure of this icy layer.

B. Goals

The goals of the HELISCAT measurements were twofold. The first one is to obtain a dataset of in situ and remotely sensed sea ice information for the Storfjorden, particularly its polynyas, in order to contribute to the evaluation of the sea ice part of micro- to meso-scale numerical ocean modelling of this area at the Institute of Oceanography, Hamburg (I. Harms). This includes detailed in-situ observations of the sea ice and snow properties on the one hand, in order to establish a data set to be used to evaluate both model and remote sensing data. And on the other hand, this includes sea ice backscatter measurements over sea ice with special emphasis on thin ice in order to improve current ice type classification schemes using satellite-based SAR imagery. The aim here is a SAR image classification scheme capable to routinely monitor the extent of polynyas in the Storfjorden area using Envisat ASAR and/or ERS2 SAR data. The second goal is to collect a data set of radar backscatter measurements for comparison/evaluation with/of Envisat ASAR imagery, and for modification of a current SAR ice classification method (L. Kaleschke, Uni Bremen). Here special emphasis will be put on as many as possible different sea ice types and surface properties. Again, these measurements will be accompanied by as many as possible in-situ observations of the sea ice and snow cover properties. For the aimed comparison/evaluation with/of SAR data only C-Band measurements are required. However the QuikSCAT Seawinds scatterometers obtains data at Ku-Band (13.4 GHz), the JERS-1 at L-Band (1.275 GHz) and the planned TERRASAR will use X-Band (9.8 GHz) for remote sensing of the surface at incidence angles within the range that is covered by the HELISCAT. Therefore it is intended to compare the data acquired with the HELISCAT at these frequencies with measurements of these sensors - at least JERS and QuickSCAT.

C. Measurements

In total 14 flights were carried out with the helicopter using the HELISCAT of which seven flights took place in the Storfjorden area/Barents Sea, and seven took place north of Svalbard. The typical flight pattern was a triangle with a total length of 60 nautical miles. This pattern was chosen in order to cover a wider area than with just a transect. Flight altitude was about 150 m for the first five flights and about 80 m for all other flights. The cruise speed changed from approximately 80 to 90 kn for the first four flights to about 100 kn during the rest of the cruise - except the tandem flight carried out on April 19. On this day the HEM-Bird (Section SEAICE.4.1.3) and the HELISCAT were flown together along the same track. Cruising speed was 60 kn in this case due to the nominal cruising speed required for the HEM-bird.

Incidence angles were usually not varied during the flight. Depending on the satellite overpass of that particular day or the day before/after (Envisat ASAR or ERS2 SAR) the incidence angle was either set to 23° in case of an ERS2-SAR overpass or to 40° in case of an Envisat-ASAR overpass. During another flight which took place during the drift station, the incidence angle was changed systematically between 60° and 20° in steps of 10° while trying to overpass the same ice area in order to have measurements at different incidence angles over the same ice type.

For all flights latitude and longitude of the flight track were acquired with a handheld GPS - at least as long receiving conditions permitted. During some flights the GPS was not able to receive data from enough satellites to provide a proper flight track. In this case the GPS of the helicopter was used to obtain at least the corner coordinates of the flight pattern. During almost all flights pictures were taken with a digital camera at locations marked with the GPS.

Helicopter speed and flight altitude were taken from the instruments of the helicopter. Starting with the seventh flight, a laser altimeter (Section SEAICE.5) was mounted on the left side of the helicopter. This vertically downward looking instrument provides the flight altitude very accurately at a sampling rate of 2 kHz. Furthermore, this altimeter allows to obtain ice ridge distribution and height accurately, which is a perfect combination to the NRCS measurements obtained with the HELISCAT.

D. Results

During all flights HELISCAT data were acquired at at least four of the five possible frequencies. Data have been stored on video tape and were subsequently digitised in the lab. It turned out already during the flights that the cold temperatures and/or the change between rather warm conditions inside the helicopter hangar and the cold conditions outside at least before/during the start have affected the reliability of some components of the HELISCAT.

A first quality check conducted on board Polarstern revealed that a) the amplifiers have caused problems during the first flights - particularly during the first part of the cruise and in C- and Ku-Band. This might be fixed later using some additional filters while re-digitising the data; b) the components are highly temperature sensitive and cause a substantial drift in the data, which, however, can be corrected for by performing the further data analysis step-by-step, assuming a rather constant temperature during shorter time intervals; c) the data acquired show a signal for all flights at least at two frequencies and that the last six flights were successful with a signal at all frequencies used during these flights.

Any further analysis will take place at the IfM in Hamburg once the equipment is back and will start with a further quality check of the already digitised data. Then the video data will be viewed and periods when the HELISCAT flew over distinct surface types (nilas with/without frost flowers, level ice, brash ice, first-year ice, multiyear ice, open water with/without grease ice) will be marked, selected and collected. On the basis of this supplementary information HELISCAT data will be analysed separately for each surface type discernible in the video in order to obtain the relative backscatter variation between different ice/surface types. The final step will be to use a sophisticated radar backscatter model developed at the University of Hamburg (R. Romeiser) to model NRCS values over open water according to HELISCAT

flight parameters and meteorological conditions encountered during HELISCAT flights over open water and by doing so to get an estimate of the absolute NRCS values.

Figures SEAICE.9, 10, and 11 show one flight track and typical backscatter profiles along this track obtained from Envisat and HELISCAT.

E. Acknowledgements

We would like to thank the crew of R/V Polarstern as well as of Wasserthal-Helicopter Service and related people for perfect collaboration. Moreover, I very much benefited from the supplementary equipment (GPS, Laser-Altimeter) which was kindly provided by the AWI sea ice geophysics group. Thanks a lot.
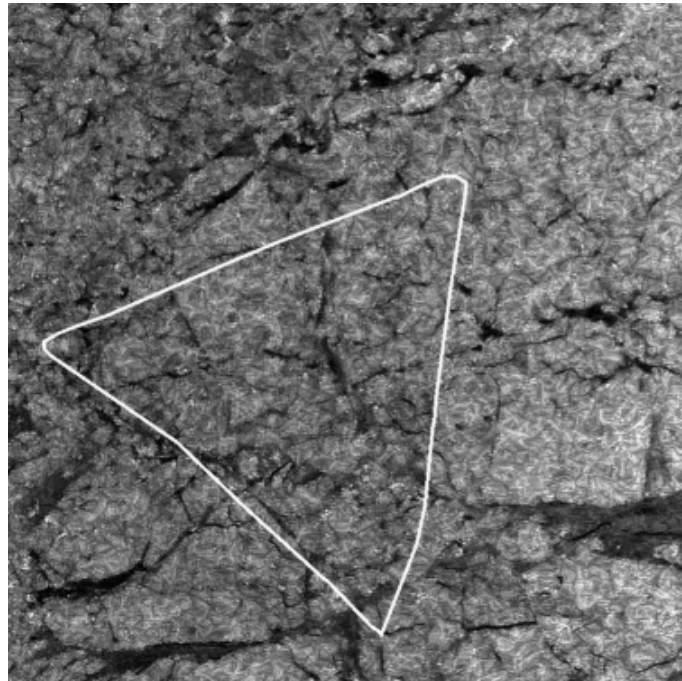

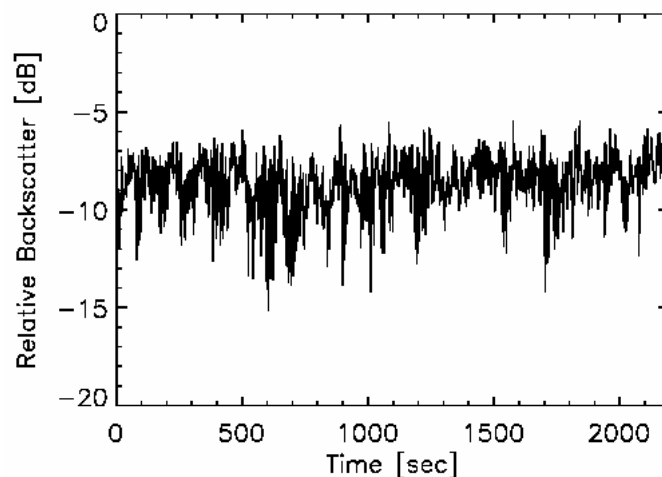**Figure SEAICE.9**: HELISCAT track on April 15, overlaid on Envisat VV SAR image.

Figure SEAICE.10: Envisat C-Band VV backscatter along flight track in Figure SEAICE.10.
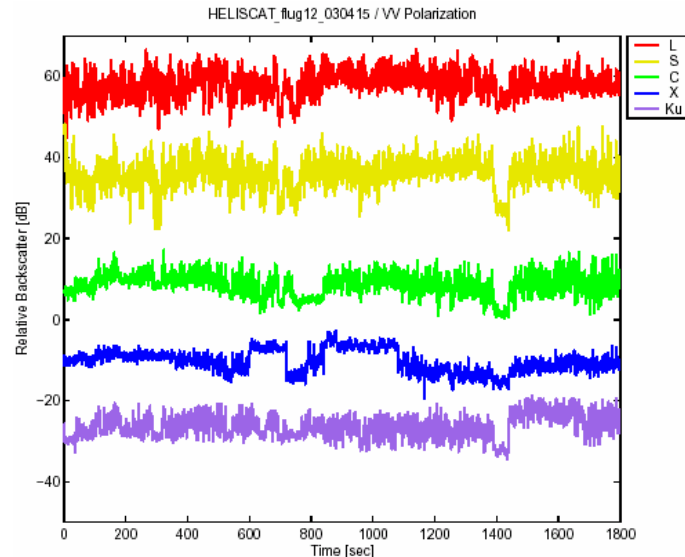
Figure SEAICE.11: HELISCAT VV backscatter along flight track in Figures SEAICE.9&10.

4. Ice thickness measurements

The main goal of ice thickness measurements was to gain high resolution data to describe local and regional thickness distributions and surface morphology. Extensive ice thickness profiling was carried out by means of electromagnetic (EM) induction sounding. The technique allows for continuous high accuracy measurements, performed either directly from the ice surface or from above, e.g. by means of the ship or helicopters.

With EM sounding, a low-frequency EM field is generated by a transmitter coil. This field induces eddy currents in the water, which in turn result in a secondary EM field. The strength of this field is measured by a receiver coil. As the strength of any EM field decreases with distance to the source, the secondary field strength decreases with increasing distance between the EM instrument and the water underneath the ice. Thus, the thicker the ice is, the weaker the secondary field becomes. Here, we deployed a hierarchy of different means of EM soundings: Ground-based measurements have proven to provide very accurate data (Section SEAICE.4.1.1). Their calibration is evaluated by means of accompanying drill-hole measurements. However, ground-based measurements are only possible on single, thick floes, and the profile lengths are very limited. Another possibility is to perform continuous ship borne measurements along the ships track. These provide the most extensive data en-route without any extra requirement for ship time (Section SEAICE.4.1.2). However, ice thicknesses along a ships track is never representative for a particular ice regime, as the ship usually follows leads with open water or new ice. At floe contacts, where the icebreaker has to break thicker ice, the ice is often deformed. Therefore we also carried out extensive helicopter borne surveys using a towed sensor, the EM bird.

4.1 Methods

4.1.1 Ground-based profiling using an EM31 thickness sensor (C. Haas)

Ground-based measurements have been performed on a daily basis on single ice floes using a Geonics EM31 instrument. Floes have been entered either from the ship or by helicopter during floe-hopping, when several floes were profiled during one flight. The EM31 operates at a frequency of 9.8 kHz with a coil spacing of 3.66 m. The EM31 provides high accuracy data and the procedures are well established. The EM31 was placed into a Prijon kayak

serving as amphibic sledge, to enable measurements over melt ponds and to shelter the instrument. EM soundings were performed at a lateral spacing of 5 m. The profiles were laid along straight lines, including level and deformed ice. The EM profiles were occasionally validated by means of drill-hole measurements when time and weather allowed.

Along the EM profiles, also snow thickness was profiled using a ruler stick. This provided essential data e.g. for CryoSat validation, as the obtained data allow to distinguish between snow and ice thickness.

4.1.2 SIMS (Sea Ice Monitoring System): Continuous along-track ice thickness measurements (C. Haas)

Since 1994, continuous EM ice thickness measurements are performed along ship tracks. Since 2001 (Ark 17/2), a Geonics EM31 is used together with a Riegl laser profiler, and the system is integrated into Polarsterns PODAS system, called SIMS. During Ark 19/1, first tests were made integrating a KT15 infrared thermometer into the SIMS. The data were acquired with the turbulence measurements at the bow, and kindly provided by W. Cohrs (AWI).

Unfortunately, archiving of SIMS data into PODAS could still not be achieved, although the data were readily visible on the ships information monitors, including those on the bridge. Therefore, the navigation (GPS) data had to be joined with the thickness soundings only during post processing. However, synchronised and georeferenced thickness, speed, and surface temperature data are available shortly after the cruise.

SIMS was operated continuously from March 09 until April 19 when Polarstern was steaming in ice. Calibration is an important duty in EM thickness profiling, and is required to asses the systems stability. In the beginning, an old calibration from 2002 was used, because no actual calibration could be performed due to the lack of extensive water patches or leads.

The first calibration was therefore only carried out on March 23, 2003. During a five minute calibration experiment, SIMS was raised and lowered in a large lead above open water, and the according laser height and EM reading (apparent conductivity) was recorded (Fig. SEAICE.12). The relationship between apparent conductivity and SIMS height above the water surface shows the well-known negative-exponential relation (Fig. SEAICE.13). The curve has a very good signal-to-noise ratio except for some scatter between 4.5 and 6.0 m, which is due to some brash ice under the system. A calibration curve can be obtained by fitting a negative-exponential function to the data (Fig. SEAICE.13). Inversion of this function yields a transformation equation to compute distance to the water surface from apparent conductivity. Ice thickness is then obtained by subtracting the laser-measured height above the ice surface.
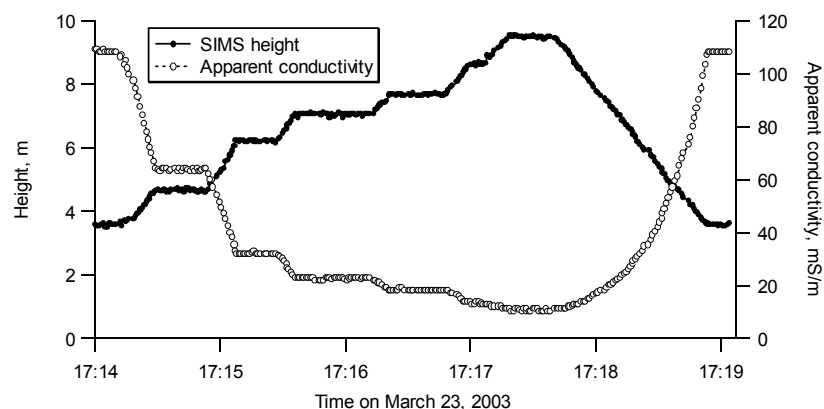

Figure SEAICE.12: SIMS height and corresponding measured apparent conductivity during a calibration measurement, when SIMS was risen and lowered over open water.

The 2003 calibration agrees with the curve of Ark 11 in 1995 (Fig. SEAICE.14), which was well explained by a one-dimensional model of a non-conductive ice cover overlying deep sea water with a conductivity of 2600 mS/m. The remaining discrepancy may be due to a different calibration factor of the particular EM31 used (e.g. a factor of 1.12 to account for instrument use at hip-height), but should be controlled by repeated calibration measurements. Deviations from the 2001 curve are quite significant, and point to an outbalanced (tilted) SIMS during 2001. The scatter of the curves demonstrates how important repeated and careful calibration measurements are. They should be performed also with future SIMS realisations.
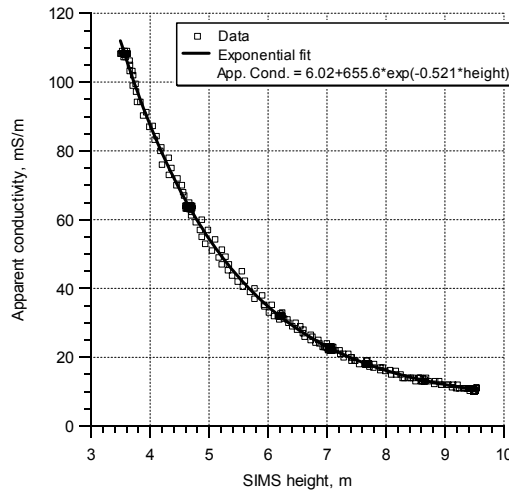

Figure SEAICE.13: Apparent conductivity (EM31 reading) versus SIMS height during the calibration measurement of Fig. SEAICE.12.
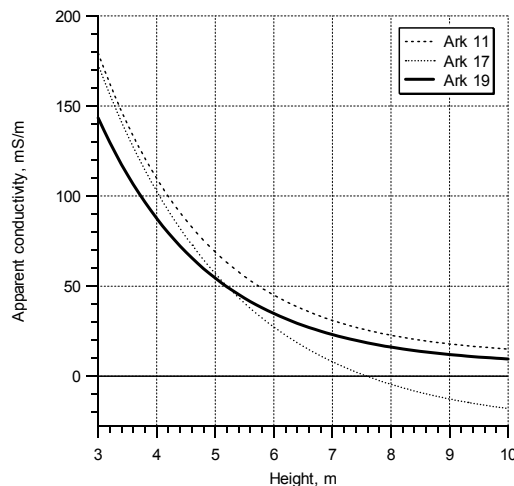

Figure SEAICE.14: Comparison of different calibration curves obtained during Ark 11 (1995), Ark 17 (2001), and Ark 19 (2003).

A typical thickness profile is shown in Figure SEAICE.15. The data were recorded during extensive ramming, showing the typical cycle of absent or thin ice and thick ice which brought the ship to a stop. Accordingly, the resulting thickness histogram shows two clear modes at 0 m and 1.6 m ice thickness (Fig. SEAICE.16). The example illustrates the importance of co-registered GPS data, if the real thickness distribution of the regions shall be derived. This can only be obtained by removing all sections of the track when the ship was moving backwards or repeating a measurement over a formerly profiled spot. In fact, the

typical thickness in the regions of the example was 1.6 m, explaining well the difficulties in straight moving forward.
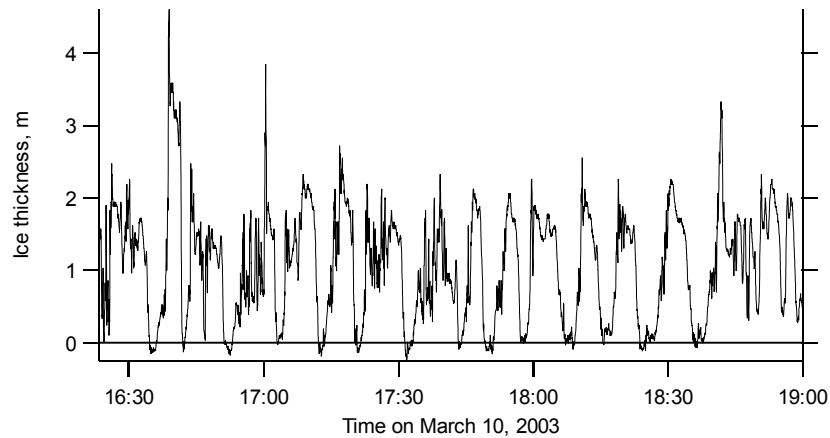

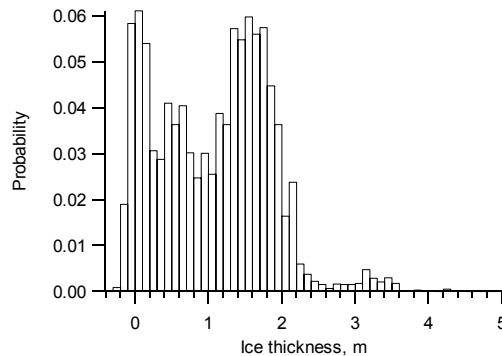**Figure SEAICE.15**: 2.5 hour recording of ramming cycles.

Figure SEAICE.16: Thickness distribution for the example in Figure SEAICE.15.

4.1.3 Airborne EM thickness profiling (C. Haas, J. Lobach, A. Pfaffling)

A helicopterborne EM ice thickness sensor (EM bird) was operated with the Polarstern BO-105 helicopters during 21 flights. The bird is 3.5 m long, has a diameter of 0.35 m, and weighs about 100 kg. It is towed 20 m below the helicopter, at a height of about 10 to 15 m above the ice surface. Take-off and landing were conducted from the helicopter deck. The bird was successfully landed directly into a special cart which could also be used for transport and storage on board.

The bird operates at 3.68 and 112 kHz, with coil spacings of 2.77 and 2.05 m, respectively. A GPS antenna and a laser altimeter are also included. Flights were performed along triangles with 40 km side length. At each turning point, the helicopter ascended to an altitude of 100 m to allow for internal calibration and nulling of the bird.

Some flights were complemented by ground validation along coincident short profiles on the longer ice stations close to the ship.

A nadir video camera was operated during all video flights to document ice conditions below the bird. However, on most flights videos were only recorded during the high altitude sections to limit the amount of video data and to document general ice conditions in the region.

Geo-referenced digital still photographs were also taken to document general ice conditions. Subsequently they were included into an html linked map projection allowing for easy geocoded image browsing.

4.1.4 Ground penetrating radar (GPR; A. Pfaffling, C. Haas)

During ARK 19/1 a RAMAC GPR instrument (MALA GeoScience) was taken to the sea ice for the first time to assess the capability of the method to contribute information on the sea ice properties particularly ice thickness (Fig. SEAICE.17).

Figure SEAICE.17: The RAMAC GPR mounted into a little Pulka.

In contrast to EM induction methods (EMI, Sections SEAICE.4.1.1-4.1.3), GPR systems use a high frequency (> 50 MHz) electromagnetic pulse comparable with a seismic explosion or air gun which travels inside the media. If there happen to be changes of the dielectric properties of the media on distinct horizons the EM pulse is partly reflected and returns to the receiver antenna of the system. An example for such a horizon would be the ice underside where the media changes from ice to water or the snow-ice interface. During a GPR survey such a wave travel experiment (shot) is recorded every cm along the profile.

Once the antenna has transmitted the EM impulse the receiver starts to acquire the returning signals for some nanoseconds. For interpretation the signal traces of every shot are plotted next to each other in a radargram (Fig. SEAICE.18). The grayscale displays the amplitude of the received waveform. After the reflected waveform of the ice underside is identified, the travel time of the wave down and up can be derived (between 20 – 30 ns in this example). With the help of drilling information or using standard values for the propagation velocity, the travel time can be converted into ice thickness. In Figure SEAICE.18 the bars represent the drilling information.

The propagation velocity depends on the dielectric permittivity of the media. The reflectivity is related to changes in the dielectric properties, determining the velocity. Apart from the wave travel velocity, the damping of the wave depends on the conductivity of the media and the antenna frequency (50 MHz up to 1.5 GHz). Damping increases with frequency and conductivity.

In Figure SEAICE.18 a dominant reflector corresponds nicely with the drilling information. A second reflector at around 10 ms maps the snow-ice interface as the antennas are pulled over the snow surface. Only were the ice gets too thick or consists of many little broken pieces it gets hard to find a reflected signal in the data. For comparison the EMI derived ice thickness for the same profile as in Figure SEAICE.18 is shown in Figure SEAICE.19. The circles represent the drilled thickness like the bars in the radargram.

Due to its wave characteristics and the small point spacing GPR provides results with higher lateral resolution and accuracy. However, dealing with high salinity ice or not level ice conditions as e.g. pressure ridges, there are problems to retrieve ice thickness information

which can be solved with the EMI method. The following table gives an overview of the acquired radar data during ARK 19/1:
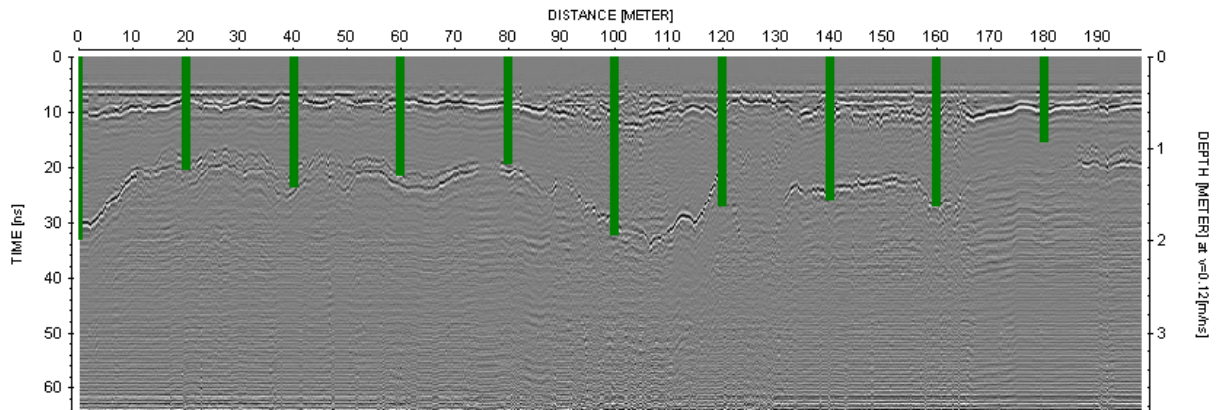

Figure SEAICE.18: GPR section (radargram), Antenna: shielded 800 MHz, Date: 20030312. Drilling information plotted as black bars.
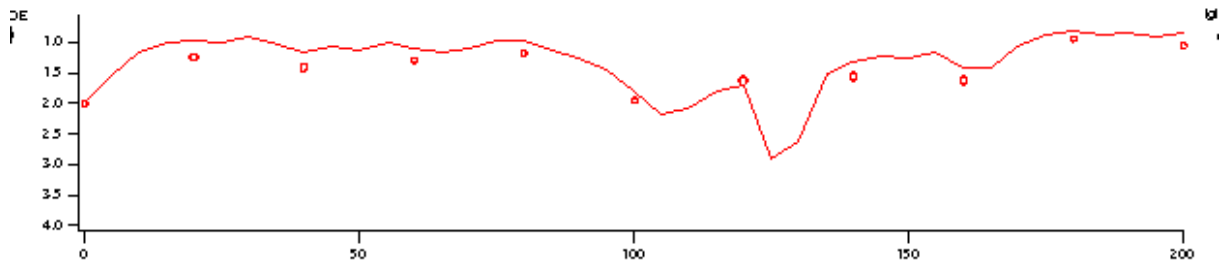

Figure SEAICE.19: EMI-derived ice thickness (lines), circles represent drilling data. Date: 20030312. Spacing: 5m.

Table SEAICE.1: GPR measurements performed on ARK 19/1. The crosses in the rows Zs and tt mark if direct snow and/or ice thickness measurements were taken on the GPR profile for validation.

Date	Zs tt	Project name	Antenna	Sampling	Profile	Remarks
12.03.2003	X X	.03031101	800 MHz	10 cm	6 m	System on snow surface
		.03031102	800 MHz	1 cm	1.5 m	All data acquired on 20030312
		.03031103	800 MHz	10 cm	3.6 m	
		.03031104	800 MHz	10 cm	200 m	
		.03031201	800 MHz	10 cm	18 m	System on Ice surface
		.03031202	800 MHz	5 cm	18 m	Profile start point equals 1m point of 030311*-profiles
17.03.2003	X X	.03031701	800 MHz	5 cm	330 m	
19.03.2003		.03031901	800 MHz	500 ms		Antenna lowered from the bow crane
		.03031902	800 MHz	500 ms		using a rope
		.03031903	800 MHz	500 ms		(Snow thickness ?)
23.03.2003	X X	.03032301	800 MHz	5 cm	200 m	System in Pulka
		.03032302	800 MHz	5 cm	200 m	System on Nansen sledge
01.04.2003	X	.03040101	1 GHz	5 cm	200 m	
07.04.2003		.03040701	800 MHz	250 ms	~ 4000 m	Joint Survey with Kayak
08.04.2003		.03040801	500 MHz	100 ms		Running chriss-chross on the floe
		.03040802	500 MHz	100 ms		to test the 500 MHz antenna
11.04.2003		.03041101	500 MHz	100 ms	2000 m	CryoVex I coincident with Kayak
13.04.2003	X X	.03041301	500 MHz	5 cm	200 m	CryoVex I 200 m subset
		.03041302	1 GHz	5 cm	200 m	Antenna on plastic box on Nansen sledge

4.2 Preliminary Results
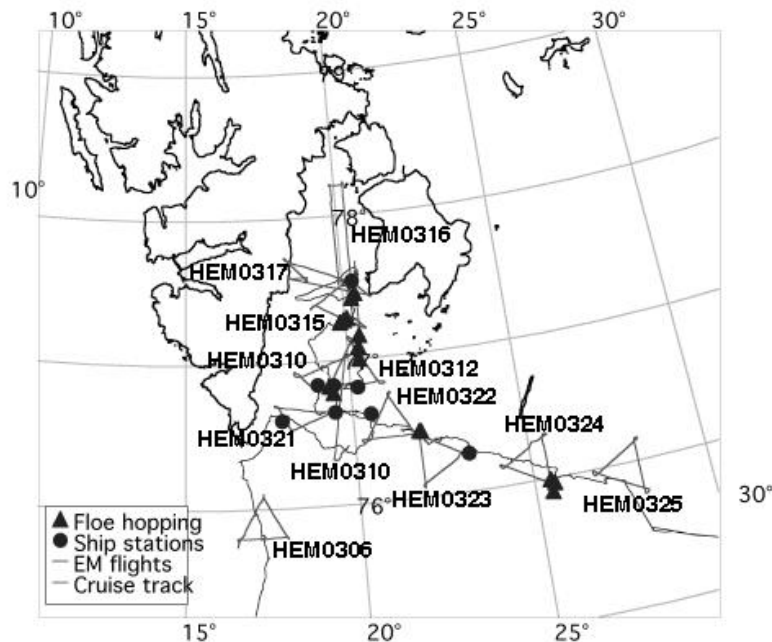
4.2.1 Storfjord and Barents Sea (C. Haas)

Figure SEAICE.20: Map of Storfjorden and Barents Sea, showing the locations of ground measurements and tracks and dates of helicopter EM flights.

By means of ground measurements and EM flights, much of the Storfjorden and an almost continuous section across the Barents Sea could be profiled. In total, we sampled 24 floes and performed 12 EM flights (Fig. SEAICE.20).

Figure SEAICE.21 shows typical ice and snow thickness obtained from ground-measurements versus latitude, i.e. a pseudo profile along Storfjorden and the neighbouring Barents Sea. In Storfjorden, no clear thickness trends from N to S are visible. However, it should be noted that due to the cruise track no measurements were possible in the first-year ice produced in Storfjorden. Typical thicknesses between 0.6 and 1.0 m are in partial agreement with the airborne thickness distributions presented below. However, it becomes clear that the ground measurements were much too sparse to be representative for the overall thickness distribution. In the Barents Sea, a gradual thinning towards the ice edge is visible. However, older and younger ice cannot be separated based on the thickness data alone.

EM flights were very well able to distinguish between the areas of thin ice formed in Storfjord and the thick ice advected from the Arctic Ocean. Figure SEAICE.22 shows a comparison of different ice thickness distributions obtained on Flights 0316 (a), 0315 (b&c), and 0312 (d), showing the transition between the different ice regimes (c.f. Fig. SEAICE.20). While the grey ice in inner Storfjorden was only 0.2 m thick, the thick ice further to the south had typical thicknesses up to 2.3 m. The modes at small thicknesses represent nilas formed on open water leads.

Figure SEAICE.23 shows the transition between the different ice regimes, which was encountered on the W-E flight on 0312. The corresponding thickness distribution is shown in Figure SEAICE.22b.
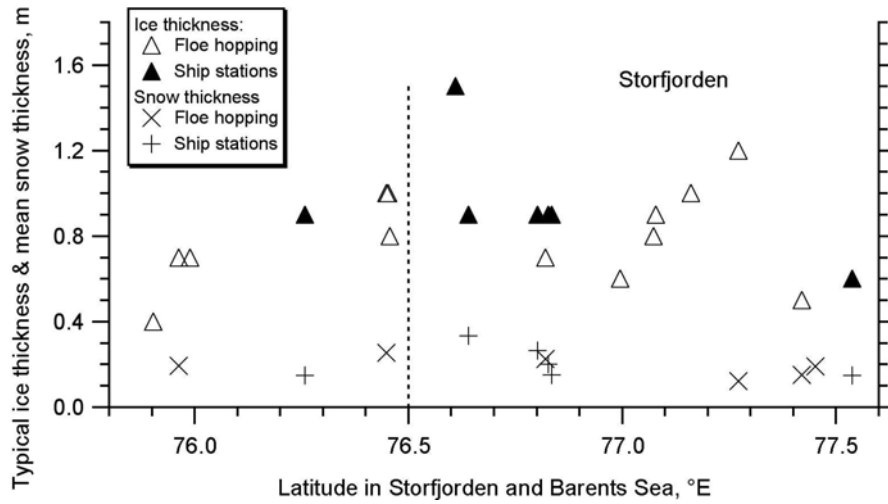
Figure SEAICE.21: Typical ice and snow thickness obtained from ground-measurements versus Latitude, between Barents Sea (left) and Storfjorden (right).
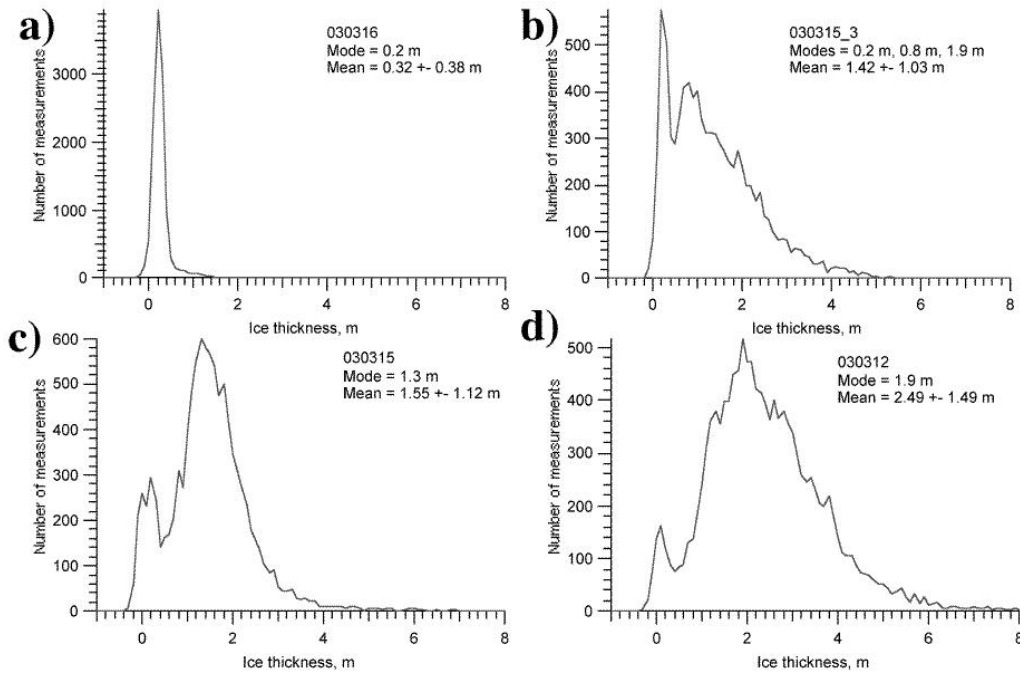

Figure SEAICE.22: Ice thickness histograms for different flights in the Storfjorden area (see text) mapping different ice regimes.
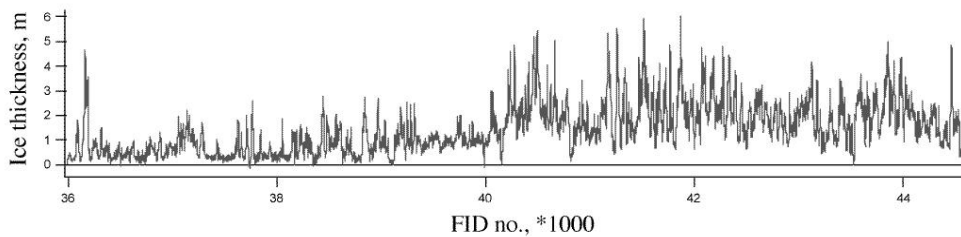

Figure SEAICE.23: Thickness profile obtained on March 12 showing the transition from thin first-year ice into thick second- or multiyear ice.

4.2.2 Fram Strait (A. Pfaffling, C. Haas)

During transit from Svalbard into Fram Strait to the drift station on the 1st April a 24 h ice station provided the possibility for a Kayak EM ice thickness profile and the weather also allowed an EM-Bird flight. A failure in the birds altitude display led to a ground contact of the system, which damaged parts of the shell. However, the excellent work of the ship's machine workshop made it possible to conduct the first test flight after the crash only three days later with the repaired bird where it turned out that all systems still worked properly. It was essential for the sea ice team as the most important part of the cruise the CryoVex 2003 campaign was about to come.

On the way back from the drift station we conducted a joint flight with the HeliSCAT system on the 19th April. Using this collocated dataset the dependency of the radar backscatter on sea ice thickness can be studied in more detail than before. Figure SEAICE.24 summarizes all flights performed in Fram Strait.
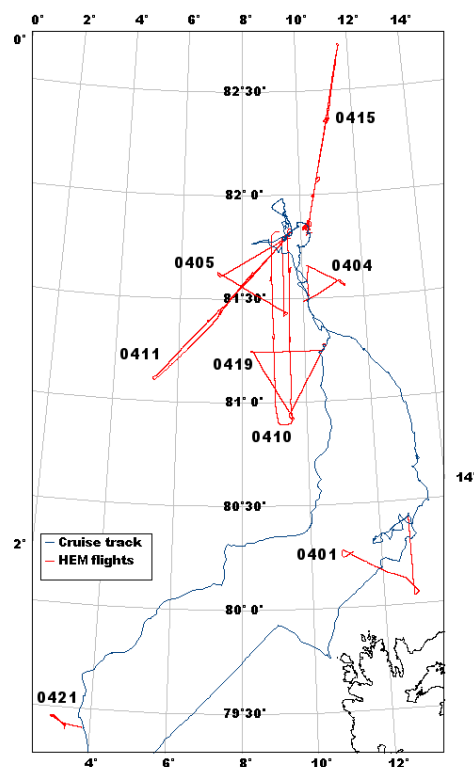

Figure SEAICE.24: Map showing HEM flight tracks during ARK 19/1b / CryoVex 2003.

4.2.3. CryoVex 2003 (A. Pfaffling, C. Haas)

The CryoSat Validation Experiment, CryoVex, is a joint effort of the AWI and the European Space Agency, ESA (in cooperation with the National Survey and Cadastre of Denmark, KMS) in order to test possible validation methods to be used on ESAs CryoSat mission.

CryoSat is ESA's first Earth Explorer Opportunity Mission and is aimed at observing changes in the Earth's cryosphere i.e. changes of the ice and snow covered parts of the Earth.

The objective of the CRYOVEX campaign is to provide reference datasets for Cryosat retrieval error studies over sea ice. In particular the campaign is aimed at understanding miscellaneous sources of error: Snow loading, ice density, preferential sampling and various freeboard measurement errors. To meet the validation requirements, the campaign goal is to collect simultaneous and coincident laserscanner / radar height measurements (from the KMS

twin otter) and HEM ice thickness profiles (from the Polarstern Helicopter) for cross-validation combined with in-situ thickness data from Kayak EM measurements and drillings (done by AWI).

During the drift station period two joint CryoVex flights were done. As a consequence of the poor flight weather conditions either on Svalbard or around Polarstern or even both it was very hard to find two suitable days. Figure SEAICE.25 shows the tracks of those flights. As the two aircrafts operate at different speeds it is important to find flight concepts to sample the same ice as the sea ice is not stationary but moves with the drift. Therefore the first flight (11th April) was aligned upstream the drift direction. Prior to the Helicopter take off the momentary drift direction and speed was determined from the Polarstern GPS data. For the second flight a heading approx. north was chosen to reach a different ice regime observed from satellite data prior to the flight.

Scale: 1:375497 at Latitude 90°
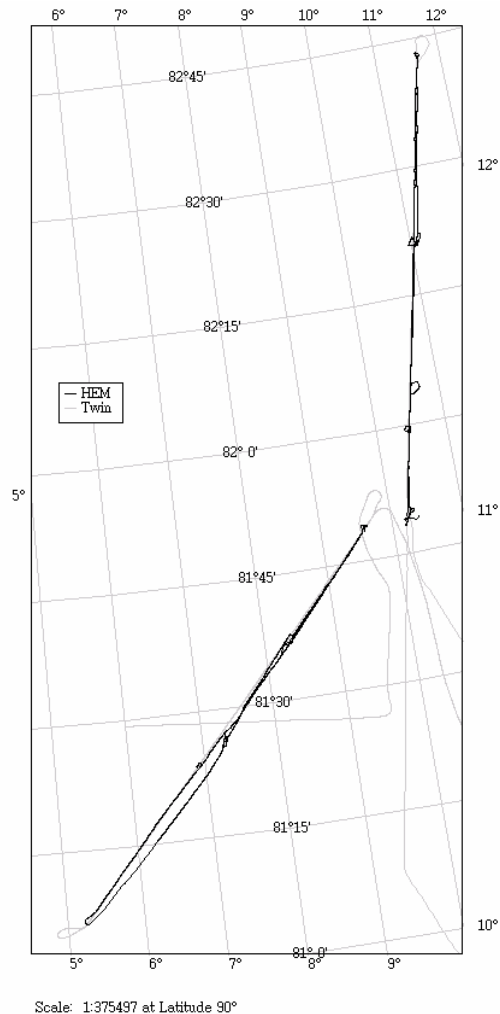
Figure SEAICE.25: Flight tracks of the two coincident CryoVex flights on 11th and 15th April. Lines marked as "Twin" indicate tracks of the Danish Laserscanner and D2P radar altimeter on board the Greenland Air Twin Otter. HEM flight lines are labeled as "HEM".

Data from CryoVex I flight on 11th April are shown in Figure SEAICE.26. For cross validation of the airborne sea ice data approx. the first 2 km of the flight track were surveyed with the sledge EM, and GPR device combined with a 200m subset of 11 drillings. The excellent agreement between the airborne and ground EM results is shown in Figure SEAICE.26a. Studying 30 of the 100 km leg in Figure SEAICE.26b thick multiyear floes can be separated form open and refrozen leads. The peaks in the curve up to ten and more meter draft indicate massive ridges within the floes.

a)

b)

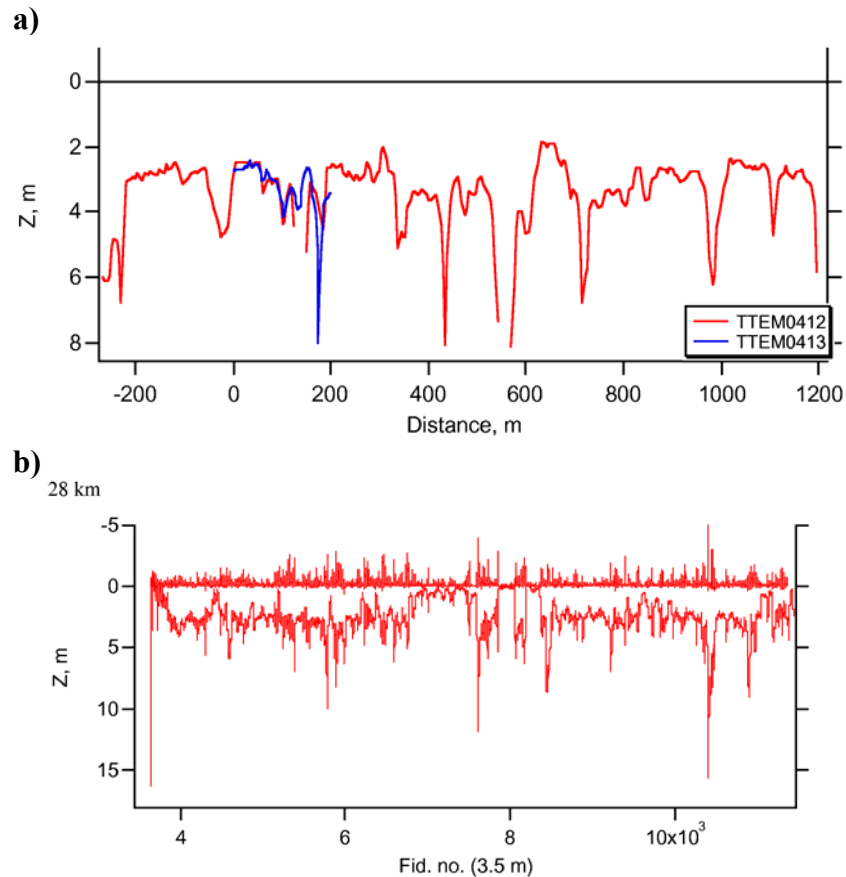**Figure SEAICE.26**: a.) subset of the HEM data of the first CryoVex flight on 11.04.2003 compared to the ice thickness derived with the sledge EM. b.) 30 km ice thickness profile obtained during the joint flight on 11th April 2003.

5. Laser profiling of pressure ridges (T. Martin, C. Haas)

Pressure ridges are the most significant features of sea ice roughness. Ice floes, which collide due to wind forcing or swell, tend to pile up in so called ridges. Ridges are separated into an upper part, the sail, and a lower part below the ice or water surface, the keel. Both features are important for momentum flux from atmosphere and ocean to the ice. Typically the keel is about 4 times deeper as the sail high and also 2-3 times wider.

The laser measurements performed with the EM bird (Section SEAICE.4.1.3) can be processed to obtain height, width and spacing of pressure ridges. During the first part of the cruise in the Storfjord region 12 and during the second part north of Svalbard and north of Fram Strait 8 helicopter flights were performed. The flight tracks ranged from 60 km to 200 km and were in most cases shaped like triangles with equally sized sides. With an intermediate flight speed of 60 knots and a sampling frequency of 100 Hz point spacing results in 0.3 m. The instrument was usually flown about 15 - 20 m above the ground.

The processing of the laser data is complicated by variably vertical motion of the helicopter. That is why the raw data has to be high pass filtered first in order to fit a curve of the helicopter movement. In a second step a profile of the surface is derived. Furthermore mean height, width and spacing of pressure ridges and their number per km along the flight track is calculated as well as width and number per km of ice floes and leads. To define individually identifiable ridges a Rayleigh criterion is used which means that a single ridge must have a crest elevation of more than double the height of the surrounding troughs.

Besides being an Arctic winter expedition this cruise features measurements of young and first year ice on the one hand and multiyear ice on the other hand. The typical difference in surface roughness as revealed by the processed laser data is shown in Figure SEAICE.27, comparing level grey ice in Storfjorden with heavily deformed multiyear ice in Fram Strait. Preliminary results show that ice floes in Fram Strait were 30 times larger in diameter than the floes in Storfjorden (100 m average). However, ridge frequency was similar in both regions, amounting to about 22 ridges per km. The smaller floes in Storfjorden allow wind and oceanic currents to produce more leads. The data show a two orders of magnitude higher number of leads in the Storfjorden compared to the Fram Strait profile.

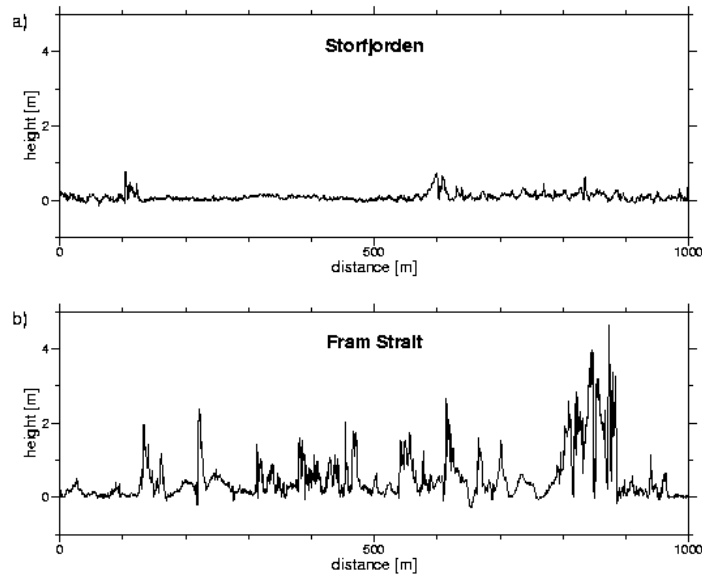

Figure SEAICE.27: Comparison of laser derived surface roughness of undeformed grey ice in Storfjorden (a) and heavily deformed multiyear ice in Fram Strait (b). The Fram Strait profile is from the first CryoVex flight.

6. Ice coring (C. Haas, S. Willmes)

Supported by the biological sea ice group 10 ice cores were obtained on different floes visited during thickness work. They were analysed for crystal texture and salinity to better judge age and origin of the sampled floes. In fact, only through these analyses a clear picture of the different young and old ice regimes arose which was not so clear based on thickness profiles alone.

Figure SEAICE.28 illustrates the typical C-shaped profiles of first year ice from the Barents Sea and the almost fresh ice typical for multiyear ice in Storfjorden. On March 16, the ice floe consisted of an old floe rafted over a first-year floe.
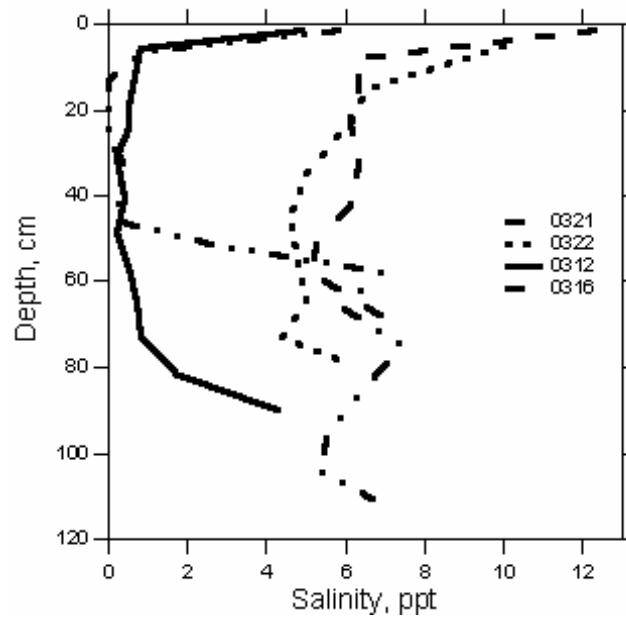

Figure SEAICE.28: Typical salinity profiles of four ice cores obtained in Storfjorden and the Barents Sea.

7. Snow measurements (V. Alexandrov)

Several key snow parameters were measured including snow density and depth. These are important for the interpretation of satellite imagery. During the ice stations snow depth was measured randomly on ice floes of different thickness. Temperature/density profiles were obtained in several snow pits using a special snow density kit.

Altogether 41 snow pits were investigated (Table SEAICE.2). These measurements were conducted on different sea ice types: thin, medium, thick first-year and multiyear ice. The temperature profiles of snow were obtained for different snow depths in the wide band from –1°C to –30°C. Snow measurements were supported with photos of ice floes, snow structure, and upper layer of the snow. Studies of typical distribution of snow density, and typical temperature profiles under different air temperatures will be done after the expedition.

Table SEAICE.2: Summary of snow measurements.

N	Date	Coordinates	Number of snow pits	Snow depth	Tair, ^{o}C
1	March 7	76° 37'N/17° 57'E	1	Yes	-18.8
2	March 8	76° 35'N/20° 37'E	1	Yes	-13.0
3	March 9	76° 38'N/19° 30'E	1	Yes	-10.7
4	March 10	76° 50'N/19° 02'E	-	Yes	-16.3
5	March 11	76° 50'N/19° 30'E	-	Yes	-26.0
6	March 12	76° 49'N/20° 13'E	2	Yes	-29.0
7	March 16	77° 33'N/20° 21'E	1	Yes	- 9.6
8	March 17	77° 33'N/20° 21'E	3	Yes	- 16.5
9	March 19	77° 17'N/20° 05'E	2	Yes	- 21.8
10	March 21	76° 49'N/19° 23'E	2	Yes	- 4.1
11	March 22	76° 27'N/21° 53'E	2	Yes	-13.8
12	March 23	76° 17'N/23° 22'E	4	Yes	-20.6
13	March 24	75° 58'N/25° 36'E	3	Yes	-19.0
14	March 25	75° 55'N/27° 01'E	1	Yes	-19.0
15	April 1	80° 26'N/12° 50'E	3	Yes	-29.6
16	April 7	81° 54'N/09° 35'E	2	Yes	-21.0; -17.0
17	April 8	81° 54'N/09° 35'E	2	Yes	-17.7; -19.0
18	April 10	81° 49'N/09° 31'E	1	Yes	-20.1
19	April 12	81° 49'N/09° 31'E	3	Yes	- 1.2
20	April 14	81° 49'N/09° 31'E	3	Yes	-7,6; -10.0
21	April 15	81° 47'N/10° 16'E	2	Yes	-13.0
22	April 17	81° 45'N/09° 55'E	2	Yes	-14.9

8. Wave measurements (V. Alexandrov)

Measurements of waves in sea ice were conducted using a wave buoy, consisting of accelerometer and tiltmeters. The objective of this work is to study the statistical characteristics of wave power spectrum/directional wave spectrum within the marginal ice zone (MIZ) with respect to time and different sites within MIZ. A Wave Buoy produced at the Christian Michelsen Research AS (Bergen, Norway) was used for these studies.

Sixteen series of wave measurements were performed during the expedition in the period from March 7 to April 15 (Table SEAICE.3).
Five short recordings of about one hour duration have been made on March 7, 8, 9,10,11 and 25. All these recordings were produced on the first-year ice. Descriptions of ice floes were documented, and photos of the buoy location and surroundings were made. Snow thickness measurements and temperature/density profiles of snow near the buoy location were done. Three recordings of several hours duration were conducted on March 12, 23, and April 1. On March 12 wave measurements were conducted during a long ice station, which took place on a big ice floe approximately 300 m wide and 1 km long with rather level surface. The estimated average thickness amounted to 70 cm. In the place, where the buoy was installed snow thickness was 30-40 cm, and ice thickness 150 cm. Later on the buoy was placed further from Polarstern, where ice thickness was 106 cm, and long-term recording was done there. On March 23 wave measurements, conducted during the long ice station, lasted approximately seven hours. Ice floe diameter was significantly more than one km, and ice thickness was about 90 cm. At the place, where buoy was located, ice thickness was 50 cm and snow depth 15 cm. On April 1 wave measurements were conducted during a long ice station, lasted about 24 hours. Two series of wave measurements were conducted. In the first point measurements lasted 4 hours 7 minutes. The buoy was deployed on rather thick ice floe of approximately 100 m in diameter, surrounded with high ridges, up to 2 meters. The snow depth was about 35 cm. Later on the buoy was replaced to level first year ice floe of 1m thickness, where snow depth was 2-3 cm. Here the 19-hour recording was done. After the buoy was switched off a crack appeared near this place, which then significantly widened up to approximately 50 m. On March 16 wave measurements have been conducted during the long ice station on a big ice floe of approximately 150 m wide and 0.6 km long with rather level surface. Ice thickness near the buoy was 67 cm, and snow depth was about 25 cm. A snow pit was taken near the buoy. The total duration of the record amounts to 20 hours.
Four recordings, each lasting approximately 2 days were conducted during the drifting stage of the expedition. Three of them, starting on April 7, 9, and 12 were done on different parts of the multiyear ice floe. Its thickness varied from 180 cm near Polarstern to 350 cm in some places. Ice surface is quite level, with small hills, but further from the ship it becomes more rough. During the first recording this ice floe turned counter clockwise in approximately twenty degrees, but later on no rotation was observed. The photos of buoy locations and surrounding areas, as well as snow measurements were done. On April 15 the buoy was placed on thin first-year ice of 45 cm thickness, which is located in 5 meters from the multiyear ice floe, and from there it was taken on April 17.

Table SEAICE.3: Summary of WAVE BUOY measurements.

Number	Date	Latitude	Longitude	Duration
1	March7,	76°37'N	17°57'E	50 min
2	March8,	76°35'N	20°37'E	1h 5 min
3	March 9	76°38'N	19°30'E	50 min
4	March 10	76°50'N	19°02'E	30 min

5	March 11	76°50'N	19°30'E	25 min
6	March 12	76°49'N	20°13'E	3h 50 min
7	March 12	76°49'N	20°13'E	23h 38min
8	March 16	77°33'N	20°21'E	20h 12 min
9	March 23	76°17'N	23°22'E	6h 52 min
10	March 25	75°55'N	27°01'E	53 min
11	April 1	80°26'N	12°50'E	4h 07 min
12	April 1	80°25'N	12°48'E	18h 45 min
13	April 7	81°54'N	09°35'E	48h 10 min
14	April 9	81°50'N	09°43'E	Approx. 48 h
15	April 12	81°51'N	09°56'E	49h 20 min
16	April 15	81°49'N	10°14'E	46h 25 min